



HAL
open science

Enhancing alpha-Fe₂O₃(0 0 0 1) surfaces reactivity through lattice-strain control

Agnes Mahmoud, Céline Dupont

► **To cite this version:**

Agnes Mahmoud, Céline Dupont. Enhancing alpha-Fe₂O₃(0 0 0 1) surfaces reactivity through lattice-strain control. Applied Surface Science, 2020, 534, pp.147605. 10.1016/j.apsusc.2020.147605. hal-03020183

HAL Id: hal-03020183

<https://hal.science/hal-03020183>

Submitted on 24 Nov 2020

HAL is a multi-disciplinary open access archive for the deposit and dissemination of scientific research documents, whether they are published or not. The documents may come from teaching and research institutions in France or abroad, or from public or private research centers.

L'archive ouverte pluridisciplinaire **HAL**, est destinée au dépôt et à la diffusion de documents scientifiques de niveau recherche, publiés ou non, émanant des établissements d'enseignement et de recherche français ou étrangers, des laboratoires publics ou privés.

Enhancing α -Fe₂O₃(0001) surfaces reactivity through lattice-strain control.

Agnes Mahmoud¹ and Céline Dupont^{1, a)}

*Laboratoire Interdisciplinaire Carnot de Bourgogne (ICB), UMR 6303 CNRS,
Université Bourgogne Franche-Comté, BP 47870, 21078 Dijon Cedex,
France*

(Dated: 12 July 2020)

In-plane strain-engineered water adsorption on Fe- and O₃-terminated α -Fe₂O₃(0001) surfaces was investigated using dispersion corrected density functional theory. We found that in order to enhance the water adsorption capacity different type of in-plane strain is needed to be applied on the two surfaces. On Fe-terminated surface increasing compressive strain facilitates water molecular adsorption. We demonstrate that this result mainly comes from the structural behavior of the outmost Fe cation on clean Fe-terminated surface. On the contrary, in-plane tensile strain favors water adsorption and dissociation on the O₃-terminated surface. We discuss in details the possible reasons of this difference between the two surfaces in terms of structural parameters. Furthermore, we found that the two surfaces can represent two competitive molecular adsorption sites at a certain tensile strain in mixed surfaces. Finally, while strain is found to have a wide influence on the dissociation of water on the O₃ termination, its effect is less pronounced on the Fe terminated one. According to our results strain-engineering on hematite surfaces represents a feasible way to enhance the reactivity.

Keywords: hematite, water adsorption, strain, density functional theory

^{a)}Electronic mail: celine.dupont@u-bourgogne.fr

I. INTRODUCTION

A great deal of research effort has been spent to find ideal materials for water splitting. Among other semiconductors, α -hematite is considered as one of the most promising candidate¹⁻³ as a photoanode for water dissociation in photoelectrochemical (PEC) devices due to its narrow bandgap (2.1 eV), low cost, abundant natural occurrence and high photochemical stability. There are however several drawbacks regarding the PEC efficiency of α -Fe₂O₃. The limitations are due to the small hole diffusion length, short excited-state life time and poor charge separation and collection efficiency. To overcome these weak points various strategies have been developed. The control of morphology is one of the proposed ways to improve the charge separation and transportation efficiency in hematite. The use of one dimensional nanostructures such as nanotubes^{4,5}, nanowires⁶⁻⁸ or nano-cauliflower structures⁹ for PEC devices showed a significant improvement in water photo-oxidation. Other attempts to assist the PEC activity are the inclusion of dopants¹⁰⁻¹⁴ and heterostructuring with other materials.¹⁵⁻¹⁸

First principles studies can offer a way to shed light on microscopic mechanisms involved in heterogeneous catalysis. Thus several theoretical studies have been devoted to investigate the water adsorption¹⁹, dissociation^{20,21} and photo-driven oxidation on pure²², defective²³⁻²⁷ and doped α -hematite surfaces.²⁸⁻³⁰ The (0001) surface is one of the most stable naturally occurring facets of α -hematite.³¹ From the possible surface terminations of such surface the single Fe- and O₃-terminations have attracted most of the computational chemists attention³²⁻³⁴, since these are the experimentally most observed surface terminations.³⁵⁻³⁹

Iron-oxide thin films were successfully grown on both conducting metal substrates^{12,38,40,41} and metal-oxide surfaces.^{42,43} The choice of the substrate is a fundamental step in thin film growth processes, since the substrate itself and the epitaxial misfit strain can influence the film physical properties.⁴⁴⁻⁴⁷ Moreover, it has been proven theoretically that an applied strain plays an important role in the interaction of water molecules with metal-oxide surfaces.^{48,49} Yang *et al.*⁴⁸ found that the in-plane tensile strain facilitates the water adsorption and decreases the dissociation barrier on rutile TiO₂(110) surface. An other theoretical investigation⁴⁹ was dedicated to strain-induced water dissociation on supported MgO(100) thin films and they observed an enhancement in reactivity towards water dissociation related to the 5.1 % expansion in MgO(100) lattice induced by the substrate.

This study also demonstrates that the main effect comes from the geometrical influence of strain, whatever the chemical nature of the support, demonstrating that charge effects are negligible. To the best of our knowledge no such study has been devoted to hematite surfaces.

The present work is therefore intended to highlight the influence of tensile and compressive strains on water adsorption and dissociation on the single Fe- and O₃-terminated surfaces of α -Fe₂O₃(0001) by means of first principle calculations. Based on the current theoretical investigation, we believe that strain engineering in hematite thin films may offer a novel strategy to improve the catalytic activity of hematite surfaces for photodriven water splitting.

II. COMPUTATIONAL DETAILS

All calculations were performed with the Vienna *ab initio* simulation package VASP.^{50,51} The electron-ion interaction was described within the projector-augmented plane-wave (PAW) method⁵² with a kinetic energy cutoff of 550 eV. Eight valence electrons were explicitly treated for Fe (3d⁷4s¹), six for O (2s²2p⁴) and one for H (1s¹). For all calculations the spin-polarized general gradient approximation (GGA) with Perdew-Burke-Ernzerhof exchange-correlation functional (PBE)⁵³ was employed. The DFT+U approach was adopted on 3d electrons of Fe using the Dudarev approach⁵⁴ with the effective parameter of $U_{eff} = 4.3$ eV in order to describe correctly the O 2*p* - Fe 3*d* charge-transfer gap in hematite.

In each 2D structures a 20 Å, vacuum layer was introduced along the *z* axis to separate two successive slabs. The Brillouin zone was sampled with a 8 x 8 x 1 Monkhorst-Pack *k*-point mesh in each slab models and to improve convergence Gaussian smearing with the smearing width of $\sigma = 0.05$ was used. For water adsorption one-sided adsorption models were considered and all atoms were allowed to relaxed. The isolated water molecule was optimized in a 20 x 20 x 20 Å, box. Structural optimization with respect to the atomic coordinates was carried out until the forces converged below 0.01 eV/Å, and the convergence threshold on total energy was set to 10⁻⁶ eV. The dispersion correction term was included through the density-dependent energy correction dDsC method.^{55,56}

The surface energies per surface area (*A*) were calculated according to the following formula:

$$\gamma = \frac{1}{2A}(E_{slab} - E_{bulk}) = \frac{1}{2A} \left[E_{slab} - \frac{1}{2} N_{Fe} \mu_{Fe_2O_3} + \left(\frac{3}{2} N_{Fe} - N_O \right) \mu_O \right]$$

where E_{slab} and E_{bulk} are the total energies of the slab and the bulk structure, respectively. The factor 2 accounts for the two identical surfaces. N_{Fe} and N_O are the number of iron and oxygen atoms in the slab, respectively. $\mu_{Fe_2O_3}$ is the chemical potential of bulk hematite per formula unit. The chemical potential of oxygen μ_O is calculated as the half of the total energy of an isolated O_2 molecule.

To characterize the interaction between the surface and the H_2O molecule, molecular adsorption energies are calculated by:

$$E_{ads}(H_2O) = E(slab + H_2O) - E(slab) - E(H_2O_{(g)})$$

where $E(slab+H_2O)$ is the total energy of the adsorbate-surface system, $E(slab)$ is the total energy of the surface before water adsorption and $E(H_2O_{(g)})$ is the total energy of the isolated gas phase H_2O molecule.

In the same way, the adsorption energy for the dissociated state is defined by:

$$E_{ads}(OH + H) = E(slab + OH + H) - E(slab) - E(H_2O_{(g)})$$

where $E(slab+OH+H)$ is the total energy of the surface system plus dissociated water.

Finally the reaction energy of water dissociation is given by:

$$\Delta E_{diss} = E_{ads}(OH + H) - E_{ads}(H_2O)$$

The optimized lattice constants of bulk α -hematite $a = b = 5.066 \text{ \AA}$ and $c = 13.868 \text{ \AA}$ are in an excellent agreement with the experimentally observed structural parameters ($a = b = 5.035 \text{ \AA}$ and $c = 13.747 \text{ \AA}$).⁵⁷ The Fe- and O_3 -terminated surfaces are composed of symmetrical slabs with 1×1 periodicity cut out from the optimized bulk structure along [0001], containing 18 and 19 atomic layers, respectively. The most stable antiferromagnetic configuration of the bulk structure were adopted to the surfaces in question (see Figure 1)

The sites for water adsorption on Fe and O_3 -terminated surfaces are reported on Figure 1. The capital letters A, B and C refer to the Fe atoms located at different depths, on top of which the initial position was taken. Full optimization of the adsorbed water molecule on hematite surfaces was carried out from these starting points.

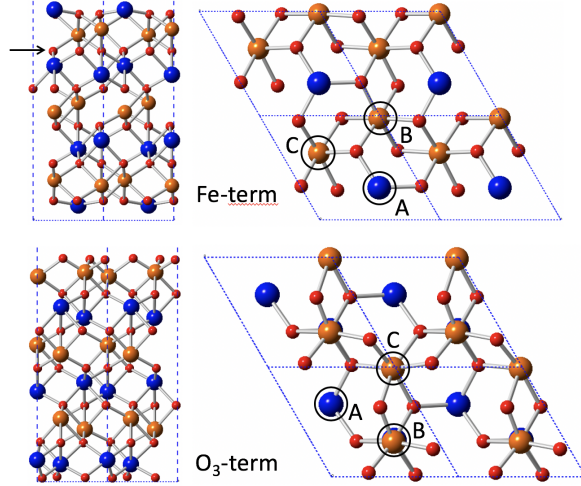


FIG. 1. Side (Left) and top views (Right) of the structural models of Fe-terminated (Top) and O_3 -terminated (Bottom) $\alpha\text{-Fe}_2\text{O}_3(0001)$ surfaces, respectively. Red spheres denote O atoms, while blue and orange spheres stand for Fe atoms, according to their magnetic state. A, B and C capital letters indicate the three studied adsorption sites, aligned on the Fe atoms of the first layers. The black arrow points out the O_3 plane used to calculate the height of the Fe surface atom.

III. RESULTS AND DISCUSSION

A. Molecular and dissociated water adsorption on unstrained $\alpha\text{-Fe}_2\text{O}_3(0001)$

Prior to any study of strain influence, molecular and dissociated adsorptions of water are considered on the unstrained Fe- and O_3 -terminated $\alpha\text{-Fe}_2\text{O}_3(0001)$ surfaces.

On the Fe-terminated surface the most favorable site for molecular water adsorption is the uncoordinated topmost Fe atom, denoted as site A on top of Figure 1. When optimization is started from the other two sites (B and C), water always evolves towards site A. Hence only this configuration will be considered in the following. It corresponds to an adsorption energy of -1.06 eV, with the water molecule bonded by its oxygen to the topmost Fe atom ($O_w\text{-Fe}_s = 2.15 \text{ \AA}$). The molecule shows a tilted configuration with respect to the surface plane due to the hydrogen bond with the neighboring surface oxygen of hematite ($H_1\text{-O}_s = 1.64 \text{ \AA}$). This hydrogen bond formation induces an elongation of $O_w\text{-H}_1$ (1.04 \AA) bond with respect to the isolated water molecule (0.97 \AA).

The O_3 -terminated surface is obtained by the removal of the topmost Fe atom from the

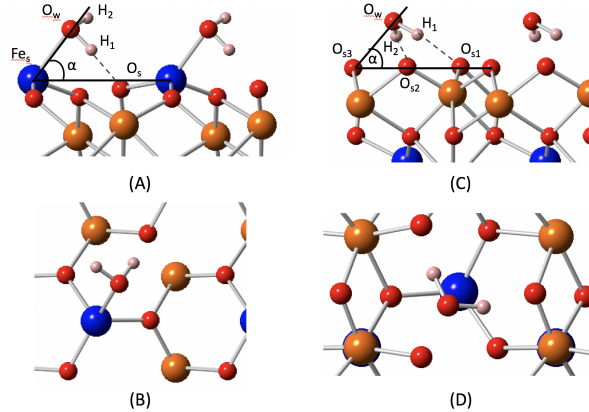


FIG. 2. (A) Side and (B) Top views of the most stable molecular adsorption configuration of water on the Fe-terminated α - $\text{Fe}_2\text{O}_3(0001)$ surface. (C) and (D) same for the O_3 -terminated α - $\text{Fe}_2\text{O}_3(0001)$ surface. O_w stands for the oxygen atom in water molecule and Fe_s , O_{s1} , O_{s2} , O_{s3} are the surface iron and oxygen atoms of hematite involved in the adsorption.

Fe-terminated surface, thus water molecule can mainly interact with the surface through hydrogen bonds. As for the Fe-termination, three different initial positions on top of the Fe atoms of the first layers (see sites A, B, and C on Figure 1 - Bottom) have been considered for the water molecule. Among the possible starting geometries site A gives the most stable configuration with an adsorption energy of -0.89 eV. This configuration is 0.27 eV more stable than the ones obtained from sites B and C. The water molecule is tilted with respect to the surface normal and attached to hematite surface oxygen by two hydrogen bonds ($\text{H}_1\text{-O}_{s1} = 1.72 \text{ \AA}$ and $\text{H}_2\text{-O}_{s2} = 1.64 \text{ \AA}$). The O-H bonds in the water molecule are only slightly stretched ($\text{O}_w\text{-H}_1 = 1.01 \text{ \AA}$, $\text{O}_w\text{-H}_2 = 1.01 \text{ \AA}$) with respect to the isolated molecule. These results are in line with previous theoretical investigations.^{20,26}

The case of dissociated water is also considered on the two terminations. As for molecular adsorption, most stable cases for both terminations are reported on Figure 3. On the Fe-termination, the $\text{Fe}_s\text{-O}_w$ bond is maintained leading to an hydroxyl group on top of the Fe_s atom. A second hydroxyl group is formed with a surface oxygen. This configuration is most stable than the molecular state, with an adsorption energy of -1.22 eV. The behavior is different on the O_3 -termination, both OH bonds of the water molecule are broken during dissociative adsorption, leading to a very stable state with an adsorption energy of -2.26

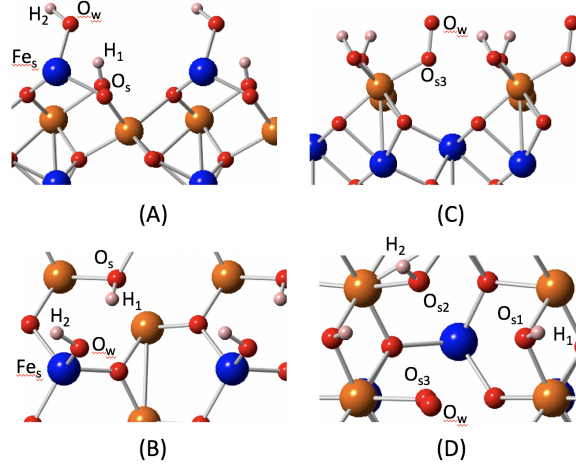


FIG. 3. (A) Side and (B) Top views of the most stable dissociated configuration of water on the Fe-terminated α -Fe₂O₃(0001) surface. (C) and (D) same for the O₃-terminated α -Fe₂O₃(0001) surface.

eV. As reported on Figure 3, two hydroxyl groups are obtained on surface oxygen atoms. Besides, an oxygen-oxygen bond is formed between O_w and O_{s3}, while no covalent bond exists in the molecular adsorbed state. The formation of this "O₂" entity is consistent with the nature of the O₃-termination, over-stoichiometric in oxygen; thus this surface looks for dioxygen formation.

B. Strain influence on bare surfaces

The influence of strain is now considered, firstly on bare surfaces. We applied in-plane strain by changing simultaneously both optimized lattice parameters in the surface plane, namely a and b, from their reference value obtained from bulk hematite (a=b=5.066 Å). Surfaces with the optimized lattice parameters of the bulk structure are taken as a reference (0 % strain). The applied strain varies from -4.0% to +5.0%, where "-" and "+" signs indicate tensile and compressive strains, respectively.

The surface energies (γ) as a function of the applied strain for Fe and O₃-terminated α -Fe₂O₃(0001) surfaces are reported on Figure 4. Over the whole strain range the Fe-terminated surface remains more stable than its O₃-terminated counterpart. From -4 % tensile strain to 0 % the surface energies of the two surfaces show a similar increasing

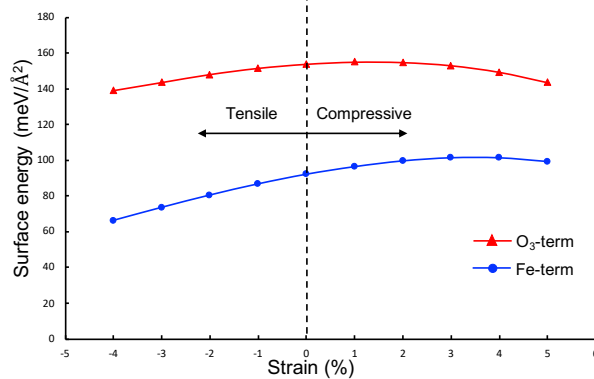


FIG. 4. Surface energies at the PBE+U level for the Fe- (blue circles) and O₃-terminated (red triangles) α -Fe₂O₃(0001) surfaces as a function of the applied strain.

quasi-linear behavior, however for Fe-terminated surface the slope is a slightly steeper. This can be directly related to the nature of the two terminations. In fact, in the Fe-terminated surface, strain has a direct influence on the behavior of the surface iron atom. As it is reported on red plot of Figure 6, the extension/compression of the lattice has a wide influence on the height of the Fe atom and thus on its stabilisation or not. On the contrary, the O₃-termination is a more open surface. As a direct consequence, the strain has less influence on this surface leading to a smoother evolution under strain. In the compressive region the trends are different. Surface energy of the O₃ termination starts to decrease at 1 %, while the surface energy maximum is reached at 3 % compressive strain for the Fe-terminated surface, followed by a slow decrease.

C. Strain influence on molecular adsorption of water

The influence of the in-plane strain on water molecular adsorption properties on Fe and O₃-terminated hematite surfaces is now investigated. Starting from our preliminary study on unstrained hematite, only site A is considered for both terminations. The adsorption energies as a function of the applied strain are reported on Figure 5. As it was already discussed, water prefers to adsorb on the uncoordinated Fe atom of Fe-terminated α -Fe₂O₃(0001) surface. From Figure 5, it clearly appears that a compressive strain enhances water adsorption on the Fe-terminated surface. On the contrary, a tensile strain reduces the water adsorption

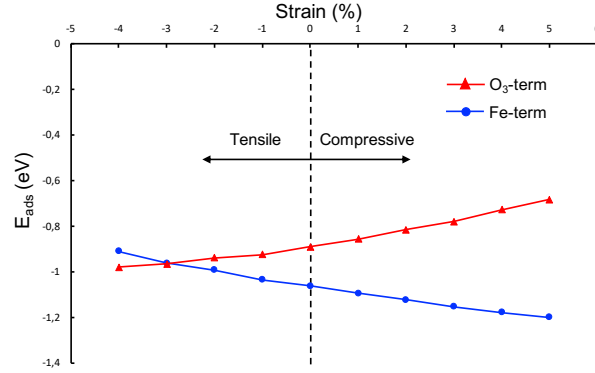


FIG. 5. Computed adsorption energies (in eV) of molecular adsorption of water on the Fe- (blue circles) and O₃-terminated (red triangles) α -Fe₂O₃(0001) surfaces as a function of the applied strain.

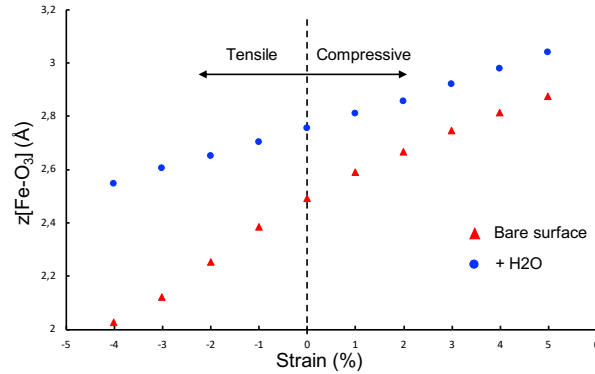


FIG. 6. Height (in Å) of the surface Fe atom in relation to the plane defined by the three oxygen atoms of the subsurface as a function of the applied strain. This plane is indicated by a black arrow on Figure 1. Red triangles correspond to the values for the bare surface, while blue circles correspond to heights after water adsorption.

efficiency on the Fe-terminated surface. The former observations can be directly supported by the geometrical changes in the hematite surface system due to the applied strains, as reported on Figure 6. This graph evidences that a compressive strain pushes the iron atom out of the surface, while for a tensile one, the top iron goes in the surface. For tensile strains of -3.0% and -4.0%, iron is even below the plane defined by the three surface oxygen atoms. This phenomenon allows to increase iron availability when the compressive strain increases. On the contrary, this iron is less accessible under tensile strain. This geometrical phenomenon explains the increasing of adsorption energy when strain evolves from -4.0% to

TABLE I. Computed equilibrium structural parameters after water adsorption in Å for distances and degree for angles (see Figure 2. (A) and (B)) at PBE+U+dDsc level for Fe-terminated α -Fe₂O₃(0001) surface as a function of the applied strain.

	Strain									
	-4.0	-3.0	-2.0	-1.0	0.0	1.0	2.0	3.0	4.0	5.0
O _w -Fe _s	2.19	2.18	2.17	2.17	2.15	2.14	2.13	2.12	2.10	2.07
H ₁ -O _s	1.84	1.74	1.72	1.70	1.64	1.60	1.57	1.52	1.47	1.39
α	52.5	51.1	50.6	50.3	50.0	49.0	48.8	48.1	47.3	46.9
O _w -H ₁	1.01	1.02	1.02	1.03	1.04	1.04	1.05	1.06	1.08	1.11
O _w -H ₂	0.98	0.98	0.98	0.98	0.98	0.98	0.98	0.98	0.97	0.97

+5.0%. Water adsorption extends this displacement of the Fe atom. However, as reported on Figure 6, the blue curve presents a lower slope than the red one. Indeed, the more the Fe atom is already out of the bare surface, the less the water has an influence.

Some other geometrical changes are induced from water adsorption, as reported in Table I. The distance between the oxygen atom of water and the surface iron of hematite (O_w-Fe_s) systematically decreases and the hydrogen-bond (H₁-O_s) between the adsorbate and the surface is also reduced within the range of -4 % to +5 %. Due to reduced hydrogen-bonds under compressive strains the bond length of O_w-H₁ in water increases, while the bond length O_w-H₂ remains almost unaffected in the whole strain range. From -4 to +5 % strain, the angle α between the water molecule and hematite surface (defined in Figure 2 (A)) is also reduced by ensuring higher adsorption energy.

Let us now describe the effect of strain on water adsorption on O₃-terminated α -Fe₂O₃(0001) surface. In this case, the situation is reversed: water adsorption is preferred on tensile surfaces (see Figure 5). However, the decrease in adsorption energy is slower for lattice expansion than its increase for the compression. As for the Fe-termination, a geometrical analysis has been performed to interpret this evolution. According to the values reported in Table II, influence of adsorption on geometrical parameters is less pronounced than on the Fe-termination. This can be directly related to the lower adsorption energies observed on the O₃-termination in relation to the different nature of adsorption. Indeed while a covalent Fe-O bond is formed during water adsorption on the Fe-termination, on the O₃ one only interactions through hydrogen bonds are observed. The only significant

TABLE II. Computed equilibrium structural parameters after water adsorption in Å for distances and degree for angles (see Figure 2. (C) and (D)) at PBE+U+dDsc level for O₃-terminated α-Fe₂O₃(0001) surface as a function of the applied strain.

	Strain									
	-4.0	-3.0	-2.0	-1.0	0.0	1.0	2.0	3.0	4.0	5.0
O _w -O _{s3}	2.13	2.13	2.12	2.12	2.12	2.14	2.13	2.14	2.16	2.17
H ₁ -O _{s1}	1.73	1.71	1.70	1.71	1.72	1.72	1.72	1.73	1.76	1.76
H ₂ -O _{s2}	1.67	1.66	1.65	1.63	1.64	1.65	1.65	1.66	1.67	1.68
α	38.8	39.8	41.2	42.6	46.0	46.3	47.2	49.1	51.0	53.2
O _w -H ₁	1.01	1.01	1.01	1.01	1.01	1.01	1.01	1.01	1.00	1.00
O _w -H ₂	1.01	1.01	1.01	1.01	1.01	1.01	1.01	1.00	1.00	1.00

evolution is observed for the α angle which increases when strain evolves from -4.0% to +5.0% expressing the evolution of the water molecule orientation towards a higher vicinity with the surface.

Let us underline one more important finding in Figure 5. In the tensile range, at -3%, there is an intersection point between the two surfaces. Hence for this strain, water could adsorbed competitively either on the Fe-termination or on the O₃ one, in case of a system with coexisting domains.

D. Strain influence on dissociative adsorption of water

The influence of strain on the dissociative adsorption is now considered. Geometries of the most stable dissociated state for each termination are reported on Figure 3 for the unstrained case, while the energetic evolution as a function of strain is presented in Figure 7

As for molecular adsorption, both terminations present two opposite behaviors. While the dissociative adsorption is facilitated by a compressive strain on the O₃-termination, a tensile one is required to favor dissociative adsorption on the Fe-termination. An other important difference comes from the range of evolution along the considered strains. On the Fe-termination, the slope is very soft, with a difference in adsorption energies of only 0.25 eV between strains of -4.0% and +5.0%. On the other hand, the slope is steeper on

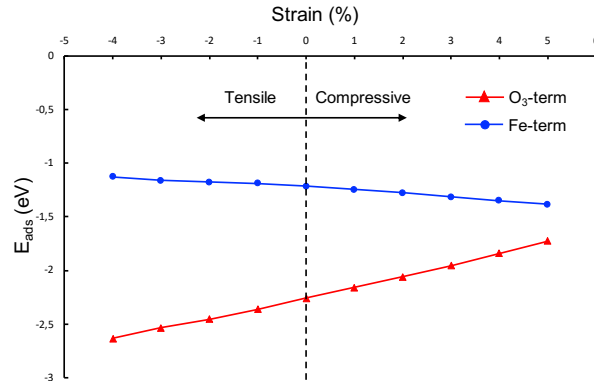


FIG. 7. Computed adsorption energies (in eV) of dissociative adsorption of water on the Fe- (blue circles) and O₃-terminated (red triangles) α -Fe₂O₃(0001) surfaces as a function of the applied strain.

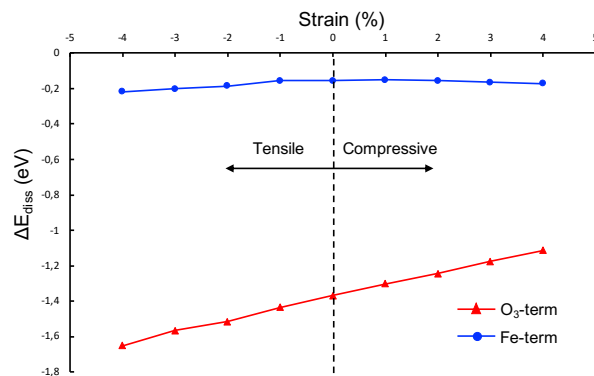


FIG. 8. Reaction energy of water dissociation on the Fe- (blue circles) and O₃-terminated (red triangles) α -Fe₂O₃(0001) surfaces as a function of the applied strain.

the O₃- termination and a difference of 0.90 eV is observed between opposite strains. Contrary to the Fe-terminated surface, no intersection is observed between the two terminations.

Finally, the ability of α -Fe₂O₃(0001) to dissociate water is considered from a thermodynamic approach. To do so, starting from previous results for molecular and dissociative adsorptions, the reaction energy of water dissociation has been calculated on both terminations and reported on Figure 8.

In keeping with previous adsorption results, both terminations present a different behavior towards dissociation. On the Fe-termination, the reaction energy is almost constant

whatever the applied strain. Indeed the dissociated state evolves like the molecular state as a function of the strain (see Figures 5 and 7). On the contrary, on the O_3 termination, when the strain evolves from the highest compressive one (5%) to the highest tensile (-4%), the stabilisation of the dissociated water molecule is more important than that of the molecular adsorbed state. Hence the reaction energy increases, and thus the dissociation of water is facilitated by a tensile strain on the O_3 -termination.

IV. CONCLUSIONS

In order to enhance the reactivity of $\alpha\text{-Fe}_2\text{O}_3(0001)$ surfaces towards water, a theory-guided strain engineering has been addressed. We found that the increasing compressive strain facilitates the molecular adsorption of water on Fe-terminated surface. The increase in adsorption energy in the compression region can be explained by the strain induced structural change in clean Fe-terminated surface. More precisely, the distance between the outmost Fe atom and the underlying O_3 plane is increased, thus the Fe atom becomes more exposed with increasing compression which increases the reactivity of the surface towards water. On the contrary, on the O_3 -terminated surface tensile strains appear to be an effective way to enhance water molecular adsorption. For a tensile strain of -3% both hematite surfaces exhibit similar binding energies, this suggests that mixed surfaces at this tensile region can have two competitive adsorption sites.

Given the ability of oxide surfaces to dissociate water, the dissociative adsorption of water has also be considered. Again both terminations present a different behavior. While dissociative adsorption is widely favored on the O_3 termination when the strain becomes more and more tensile, the strain effect is reversed and less pronounced on the Fe-termination. This has direct consequences on the reaction energy of water dissociation. In particular on the O_3 -termination, water dissociation is favored by increasing the tensile strain. These results are essential to consider strain engineering. By choosing a suitable epitaxial substrate, one can modulate the surface reactivity of hematite towards water.

V. ACKNOWLEDGEMENTS

Calculations were performed using HPC resources from DNUM CCUB (Centre de Calcul de l'Université de Bourgogne). This work was also granted access to the HPC resources of IDRIS under the allocation 2019-A0070811108 made by GENCI. The authors also thanks the ANR for financial support through projects ANR-15-CE05-PHOTO-POT and ANR-17-EURE-0002 (EIPHI Graduate School).

REFERENCES

- ¹K. Sivula, F. Le Formal, and M. Grätzel, *ChemSusChem* **4**, 432 (2011).
- ²C. Jiang, S. Moniz, A. Wang, T. Zhang, and J. W. Tang, *Chem. Soc. Rev.* **46**, 4645 (2017).
- ³R. Liu, Z. Zheng, J. Spurgeon, and X. Yang, *Energy Environ. Sci.* **7**, 2504 (2014).
- ⁴S. K. Mohapatra, S. E. John, S. Banerjee, and M. Misra, *Chem. Mater.* **21**, 3048 (2009).
- ⁵C. Li, A. Li, Z. Luo, J. Zhang, X. Chang, Z. Huang, T. Wang, and J. Gong, *Angewandte Chemie* **129**, 4214 (2017).
- ⁶Y. Ling, G. Wang, D. A. Wheeler, J. Z. Zhang, and Y. Li, *Nano Lett.* **11**, 2119 (2011).
- ⁷S. Ramadurgam, T.-G. Lin, and C. Yang, *Nano Lett.* **14**, 4517 (2014).
- ⁸P. Tang, H. Xie, C. Ros, L. Han, M. Biset-Peiro, Y. He, W. Kramer, A. P. Rodriguez, E. Saucedo, J. R. Galan-Mascaros, et al., *Energy Environ. Sci.* **10**, 2124 (2017).
- ⁹A. Kay, I. Cesar, and M. Grätzel, *J. Am. Chem. Soc.* **128**, 15714 (2006).
- ¹⁰Y.-S. Hu, A. Kleiman-Shwarscstein, A. J. Forman, D. Hazen, J.-N. Park, and E. W. McFarland, *Chem. Mater.* **20**, 3803 (2008).
- ¹¹A. Kleiman-Shwarscstein, Y.-S. Hu, A. J. Forman, G. D. Stucky, and E. W. McFarland, *J. Phys. Chem. C* **112**, 15900 (2008).
- ¹²H. Magnan, D. Stanescu, M. Rioult, E. Fonda, and A. Barbier, *Appl. Phys. Lett.* **101**, 133908 (2012).
- ¹³C. Miao, T. Shi, G. Xu, S. Ji, and C. Ye, *ACS Appl. Mater. Interfaces* **5**, 1310 (2013).
- ¹⁴R. Zhang, L. Yang, X. Huang, T. Chen, F. Qu, Z. Liu, G. Du, A. M. Asiri, and X. Sun, *J. Mater. Chem. A* **5**, 12086 (2017).
- ¹⁵X. Yang, R. Liu, C. Du, P. Dai, Z. Zheng, and D. Wang, *ACS Appl. Mater. Interfaces* **6**, 12005 (2014).

- ¹⁶C. X. Kronawitter, L. Vayssieres, S. Shen, L. Guo, D. A. Wheeler, J. Z. Zhang, B. R. Antoun, and S. S. Mao, *Energy Environ. Sci.* **4**, 3889 (2011).
- ¹⁷O. Neufeld, N. Yatom, and M. Caspary Toroker, *ACS Catalysis* **5**, 7237 (2015).
- ¹⁸W. Luo, T. Yu, Y. Wang, Z. Li, J. Ye, and Z. Zou, *J. Phys. D: Appl. Phys.* **40**, 1091 (2007).
- ¹⁹S. Yin, X. Ma, and D. Ellis, *Surf. Sci.* **601**, 2426 (2007).
- ²⁰M.-T. Nguyen, N. Seriani, and R. Gebauer, *J. Chem. Phys.* **138**, 194709 (2013).
- ²¹H. Pan, X. Meng, and G. Qin, *Phys. Chem. Chem. Phys.* **16**, 25442 (2014).
- ²²M.-T. Nguyen, N. Seriani, S. Piccinin, and R. Gebauer, *J. Chem. Phys.* **140**, 064703 (2014).
- ²³S. Yin and D. Ellis, *Surf. Sci.* **602**, 2047 (2008).
- ²⁴A. Hellman, B. Iandolo, B. Wickman, H. Grönbeck, and J. Baltrusaitis, *Surf. Sci.* **640**, 45 (2015).
- ²⁵M.-T. Nguyen, S. Piccinin, N. Seriani, and R. Gebauer, *ACS Catal.* **5**, 715 (2015).
- ²⁶R. Ovcharenko, E. Voloshina, and J. Sauer, *Phys. Chem. Chem. Phys.* **18**, 25560 (2016).
- ²⁷F. R. Negreiros, L. S. Pedroza, F. L. Souza, and G. M. Dalpian, *Phys. Chem. Chem. Phys.* **19**, 31410 (2017).
- ²⁸P. Liao, J. A. Keith, and E. A. Carter, *J. Am. Chem. Soc.* **134**, 13296 (2012).
- ²⁹M. C. Toroker, *J. Phys. Chem. C* **118**, 23162 (2014).
- ³⁰O. Neufeld and M. C. Toroker, *J. Phys. Chem. C* **119**, 5836 (2015).
- ³¹R. J. Lad and V. E. Henrich, *Surf. Sci.* **193**, 81 (1988).
- ³²X.-G. Wang, W. Weiss, S. K. Shaikhutdinov, M. Ritter, M. Petersen, F. Wagner, R. Schlögl, , and M. Scheffler, *Phys. Rev. Lett.* **81**, 1038 (1998).
- ³³X. Huang, S. K. Ramadugu, and S. Mason, *J. Phys. Chem. C* **120**, 4919 (2016).
- ³⁴A. Mahmoud, P. Deleuze, and C. Dupont, *J. Chem. Phys.* **148**, 204701 (2018).
- ³⁵S. Chambers and S. Yi, *Surf. Sci.* **439**, L785 (1999).
- ³⁶S. Thevuthasan, Y. Kim, S. Yi, S. Chambers, J. Morais, R. Denecke, C. Fadley, P. Liu, T. Kendelewicz, and G. Brown, *Surf. Sci.* **425**, 276 (1999).
- ³⁷S. Shaikhutdinov and W. Weiss, *Surface Science* **432**, L627 (1999).
- ³⁸S. Liu, S. Wang, J. Guo, and Q. Guo, *RSC Adv.* **2**, 9938 (2012).
- ³⁹G. Ketteler, W. Weiss, and W. Ranke, *Surf. Rev. Lett.* **08**, 661 (2001).

- ⁴⁰A. Barbier, R. Belkhou, P. Ohresser, M. Gautier-Soyer, O. Bezencenet, M. Mulazzi, M.-J. Guittet, and J.-B. Moussy, *Phys. Rev. B* **72**, 245423 (2005).
- ⁴¹F. Genuzio, A. Sala, T. Schmidt, D. Menzel, and H.-J. Freund, *J. Phys. Chem. C* **118**, 29068 (2014).
- ⁴²Y. Kim, Y. Gao, and S. Chambers, *Surf. Sci.* **371**, 358 (1997).
- ⁴³S. Gota, E. Guiot, M. Henriot, and M. Gautier-Soyer, *Phys. Rev. B* **60**, 14387 (1999).
- ⁴⁴H. W. Jang, S. H. Baek, D. Ortiz, C. M. Folkman, R. R. Das, Y. H. Chu, P. Shafer, J. X. Zhang, S. Choudhury, V. Vaithyanathan, et al., *Phys. Rev. Lett.* **101**, 107602 (2008).
- ⁴⁵S. Y. Zhou, G.-H. Gweon, A. V. Fedorov, P. N. First, W. A. de Heer, D.-H. Lee, F. Guinea, A. H. Castro Neto, and A. Lanzara, *Nat. Mater.* **6**, 770 (2007).
- ⁴⁶A. S. Rodin, A. Carvalho, and A. H. Castro Neto, *Phys. Rev. Lett.* **112**, 176801 (2014).
- ⁴⁷W. S. Yun and J. D. Lee, *J. Phys. Chem. C* **119**, 2822 (2015).
- ⁴⁸L. Yang, D.-J. Shu, S.-C. Li, and M. Wang, *Phys. Chem. Chem. Phys.* **18**, 14833 (2016).
- ⁴⁹Z. Song, J. Fan, and H. Xu, *Sci. Rep.* **6**, 22853 (2016).
- ⁵⁰G. Kresse and J. Furthmüller, *Comput. Mater. Sci.* **6**, 15 (1996).
- ⁵¹G. Kresse and J. Furthmüller, *Phys. Rev. B* **54**, 11169 (1996).
- ⁵²G. Kresse and D. Joubert, *Phys. Rev. B* **59**, 1758 (1999).
- ⁵³J. P. Perdew, K. Burke, and M. Ernzerhof, *Phys. Rev. Lett.* **77**, 3865 (1996).
- ⁵⁴S. L. Dudarev, G. A. Botton, S. Y. Savrasov, C. J. Humphreys, and A. P. Sutton, *Phys. Rev. B* **57**, 1505 (1998).
- ⁵⁵S. N. Steinmann and C. Corminboeuf, *J. Chem. Phys.* **134**, 044117 (2011).
- ⁵⁶S. N. Steinmann and C. Corminboeuf, *J. Chem Theory Comput.* **7**, 3567 (2011).
- ⁵⁷L. W. Finger and R. M. Hazen, *J. Appl. Phys.* **51**, 5362 (1980).